Extending the Dynamic Range of an S-Band Radar for Cloud and Precipitation Studies

ALLEN B. WHITE

Cooperative Institute for Research in Environmental Sciences, University of Colorado, and NOAA/Environmental Technology Laboratory, Boulder, Colorado

JAMES R. JORDAN, BROOKS E. MARTNER, F. MARTIN RALPH, AND BRUCE W. BARTRAM

NOAA/Environmental Technology Laboratory, Boulder, Colorado

(Manuscript received 27 September 1999, in final form 14 December 1999)

ABSTRACT

A new S-band vertical profiler with a coupler option for extending the dynamic range of the radar's receiver is discussed. The added dynamic range allows the profiler to record radar reflectivity measurements in moderate to heavy precipitation that otherwise would not have been possible with this system because of receiver saturation. The radar hardware, signal processor, and operating software are based on existing S-band and UHF profiler technology. Results from a side-by-side comparison with a calibrated Ka-band radar are used to determine the calibration and sensitivity of the S-band profiler. In a typical cloud profiling mode of operation, the sensitivity is -14 dBZ at 10 km. Examples taken from a recent field campaign are shown to illustrate the profiler's ability to measure vertical velocity and radar reflectivity profiles in clouds and precipitation, with particular emphasis on the benefit provided by the coupler technology.

1. Introduction

In general, a radar's sensitivity to small particulates increases as the transmitted wavelength, λ, decreases and as transmitted power, antenna size, beam sample volume size, and integration time increase. Similar arguments can be made for backscatter from clear-air turbulence, keeping in mind the much weaker wavelength dependence that exists in this scattering regime. Although the Rayleigh λ^{-4} backscattering dependence favors the use of shorter wavelength radars for cloud observations, even longer wavelength radars, such as UHF wind profilers ($\lambda \sim 33$–75 cm) have demonstrated some ability to detect clouds (Orr and Martner 1996; White et al. 1996). The main advantage of short-wavelength systems such as millimeter-wave radars (e.g., Moran et al. 1998) is their ability to obtain excellent sensitivity and spatial resolution without the use of large antennas or very powerful transmitters. Also, ground clutter is less of an issue at shorter wavelengths (Kropfli and Kelly 1996). Their primary disadvantage is severe attenuation by rain (but not by snow).

Operational precipitation surveillance has long been the province of centimeter-wavelength radars in the United States. Recently, the National Oceanic and Atmospheric Administration (NOAA) Aeronomy Laboratory combined wind profiler technology with S-band ($\lambda = 10$ cm) radar hardware to create a new precipitation profiler (Ecklund et al. 1999). These profilers have amply demonstrated an ability to continuously monitor precipitation echoes overhead and have also indicated a substantial ability to observe at least the more strongly reflecting regions of clouds. The enhanced sensitivity necessary for cloud profiling is achieved by coherently integrating the received signals and by pulse coding the transmitted pulses to boost the average signal power.

In this regard, an S-band profiler bridges the gap that exists between millimeter-wave cloud radars, which reveal the structure of extremely weak, nonprecipitating clouds but are severely attenuated by rainfall, and operational weather radars, which, although unattenuated by rain, generally lack the sensitivity to detect much cloud structure. This article describes a new S-band profiler built by the NOAA Environmental Technology Laboratory (ETL) that uses a switchable microwave coupler to extend the profiler's dynamic range in order to bridge this gap even more thoroughly. After a brief description of the radar and how it was calibrated, examples from recent field experiments are shown to elucidate the profiler's measurement capabilities.

2. Radar description

The prototype for the ETL S-band profiler was built at the NOAA Aeronomy Laboratory (Ecklund et al.

Corresponding author address: Dr. Allen B. White, NOAA/ETL, R/ET7, 325 Broadway, Boulder, CO 80303-3328.
E-mail: awhite@etl.noaa.gov

TABLE 1. S-band profiler characteristics.

Frequency (GHz)	2.875
Antenna diameter (m)	2.4
Average transmit power (W)	20
Peak power (W)	360
Beamwidth (deg)	2.5
Range resolution (m)	45, 60, 105, 420
Time resolution, nominal (s)	30
Doppler technique	FFT
Estimated sensitivity (dB*Ze* at 10 km)	−14

1999). The ETL profiler uses a different antenna feed that consists of a rectangular waveguide and a splash plate. The splash plate is welded to the top of the waveguide without any other supporting structure. The dish is fully illuminated, resulting in a one-way, 2.5° beamwidth (full-width at half-maximum power). Additional characteristics of the profiler are listed in Table 1. Excluding the paraboloid antenna, much of the design of the radar hardware and signal processing software is based on the existing technology used in the 915-MHz wind profilers (Carter et al. 1995).

The radar receiver uses 8-bit, in-phase, and quadrature digital converters, which limit its dynamic range to 45 dB. Doppler signal processing adds an additional 22 dB. Therefore, the total dynamic range of the profiler is 67 dB. We have detected this range in the laboratory using a sinusoidal signal, but the dynamic range apparent in field measurements will always be less. The primary reason is that the probability density function for the intensity (or power) of atmospheric signals (in clear air and in precipitation) is exponential. This makes the concept of a saturation threshold somewhat ambiguous because, for a finite dwell time, some of the instantaneous signals will saturate the receiver.

We added a switchable, 30-dB coupler to the receiver to extend the dynamic range of the ETL S-band profiler. A coupler is a microwave device that allows most of the power to pass through one port, called the through port, with little attenuation. A small amount of the power (one thousandth, in this case) traveling in the forward direction is diverted to a second port, called the coupled port. We placed the coupler and a switch, to select between the through port and the coupled port, before the first low-noise amplifier in the receiver (see Fig. 1). This configuration adds only 0.2 dB of loss to the receiver. The receiver noise level changes by about 10% when switching between the coupled mode and the noncoupled mode. Accordingly, we can switch between modes without recalibrating the receiver.

The microwave coupler and switch are simple and relatively inexpensive additions to the radar receiver. Yet we are unaware of any other attempts to use this technology to increase the dynamic range of a meteorological radar, making the coupler a unique feature of the ETL S-band profiler. Another option for increasing dynamic range is to use a logarithmic receiver. This method increases dynamic range but sacrifices sensitivity unless an additional linear receiver is sampled. By programming the S-band profiler to alternate between coupled and noncoupled operating modes, the dynamic range is increased using a single receiver and without sacrificing sensitivity.

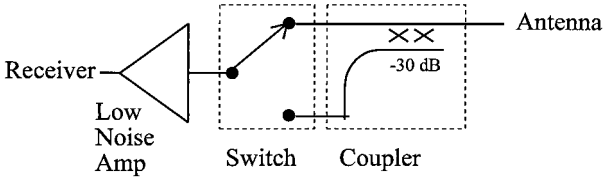

FIG. 1. Schematic of the switchable 30-dB microwave coupler used with the ETL S-band profiler. With the switch in the closed position (shown), the through port is sampled, and the signal enters the receiver without attenuation. With the switch in the open position, the coupled port is sampled, and the signal is attenuated by ~30 dB before entering the receiver.

3. System calibration and sensitivity

a. Coupler calibration

We calibrated the coupler in the laboratory by injecting a sinusoidal signal of known amplitude at the input of the radar's receiver and measuring the signal-to-noise ratio (SNR) at the output of the radar's signal processor. Tests were performed with and without the coupler. The results of the calibration are summarized in Fig. 2. The curves delimit approximately the linear response range of the receiver for the coupled and noncoupled modes. The noise floor is the output measured without any signal injected, which is a function of the

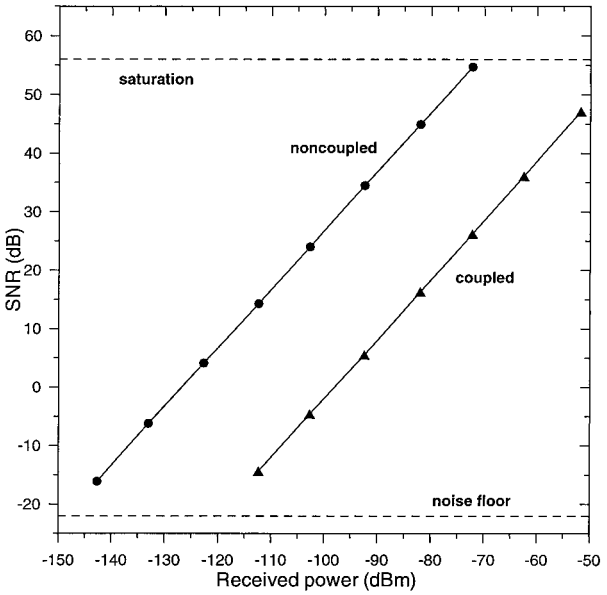

FIG. 2. Results of the coupler calibration conducted in the laboratory with the ETL S-band profiler. The received power is the signal injected at the input to the receiver. The SNR is taken at the output of the signal processor.

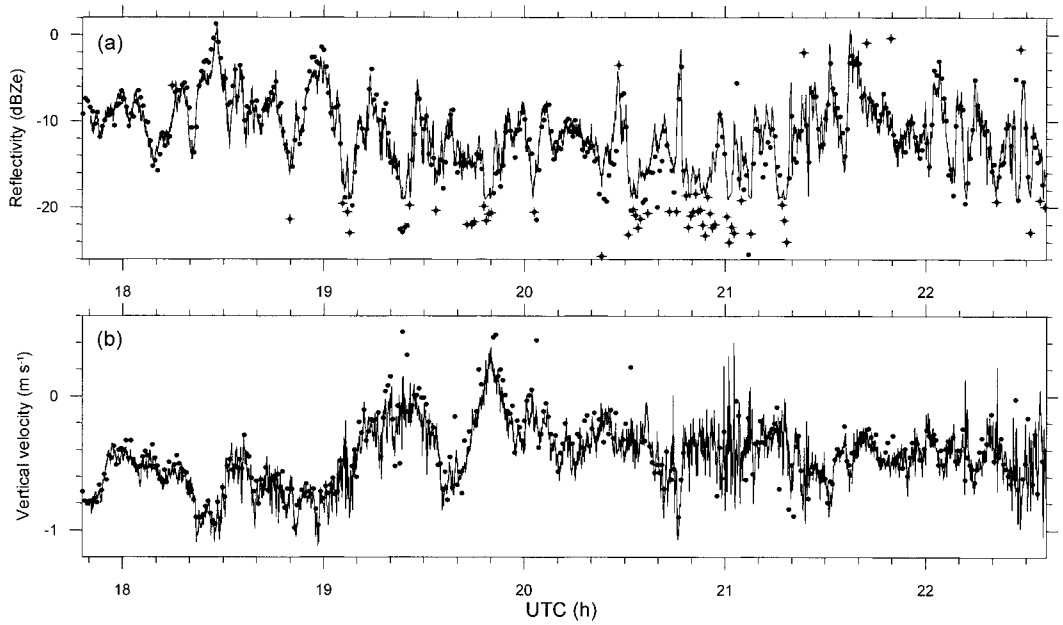

FIG. 3. (a) Equivalent radar reflectivity factor (dBZe) and (b) vertical velocity measured by the NOAA Ka-band radar (line) and the ETL S-band profiler (dots) at Erie, CO, on 8 Nov 1997. Dots with plus symbols indicate reflectivities with corresponding vertical velocities that fall outside of the range used in (b). The measurements were taken at 7 km AGL within a cirrus layer. The Ka-band radar used 37.5-m range gates, a 2.5-s sampling period, and pulse-pair signal processing. The profiler used 105-m range gates with an 8-bit pulse code, a 42-s sampling period, and spectral signal processing.

signal processing parameters used to generate the output and of ambient conditions in the field (e.g., sky noise). Therefore, the operational noise floor may be several decibels different from the value shown in Fig. 2. Over the linear response range common to both modes, the outputs are separated, on average, by 28.7 dB, indicating the actual increased dynamic range supplied by the coupler/switch mechanism for the S-band receiver.

b. Radar calibration and sensitivity

We conducted side-by-side comparisons with the ETL S-band profiler and the NOAA Ka-band radar operated in a vertically pointing mode. The latter is a highly sensitive (-30 dBZ at 10 km) millimeter-wavelength ($\lambda = 8.7$ mm) radar with a 1.2-m parabolic antenna and an offset Cassegrain feed producing a beamwidth of 0.5°. The beam is sampled with 37.5-m range resolution. The Ka-band radar has dual polarization and full scanning capabilities. Doppler velocity is calculated by the pulse-pair method, which reduces the time required for sampling compared to the spectral processing method used with the S-band profiler. A typical beam-averaging time for this radar is 0.3–3 s. Further details are given by Kropfli et al. (1995). The NOAA Ka-band radar has been extensively calibrated, and its reflectivity values are regarded as accurate to within ± 2 dBZ. Relying on ETL's long experience with this radar, we use it here as a reference for assessing the calibration and sensitivity of the S-band profiler. Unfortunately, the Ka-band radar's linear receiver malfunctioned during the brief time available for comparisons, so reflectivity data from its logarithmic receiver, which is about 10 dB less sensitive, are used in the calibration.

The comparisons were conducted at Erie, Colorado, on 30 October and 8 November 1997. On 8 November, a cirrus layer between 6 and 8 km above ground level (AGL) persisted for several hours above the observing site. To calibrate the profiler, we used the relation $Z = c_1 c_2 R^2$ SNR, where Z is the radar reflectivity factor, R is the range, and c_2 contains known constants and radar parameters and accounts for losses in the radar hardware. The Z values from the profiler and radar at selected range gates were compared to determine the calibration constant, c_1. For the operating parameters used in this study, $c_1 c_2 \simeq 1.37 \times 10^{-35}$ m. Figure 3 compares time series of calibrated effective radar reflectivity factor (dBZe) and vertical velocity from the profiler and radar taken from one selected altitude within the cloud layer.

In a quantitative comparison of backscatter data from the radar and profiler for calibration purposes, it is important to avoid heights and times when rain is present because of the severe attenuation that rainfall causes at Ka band. The routinely calculated Ka-band reflectivities may also be inaccurate if large particles are present because of non-Rayleigh backscattering effects. Thus, for the comparison it is also best to restrict the data to points where reflectivities are low because large parti-

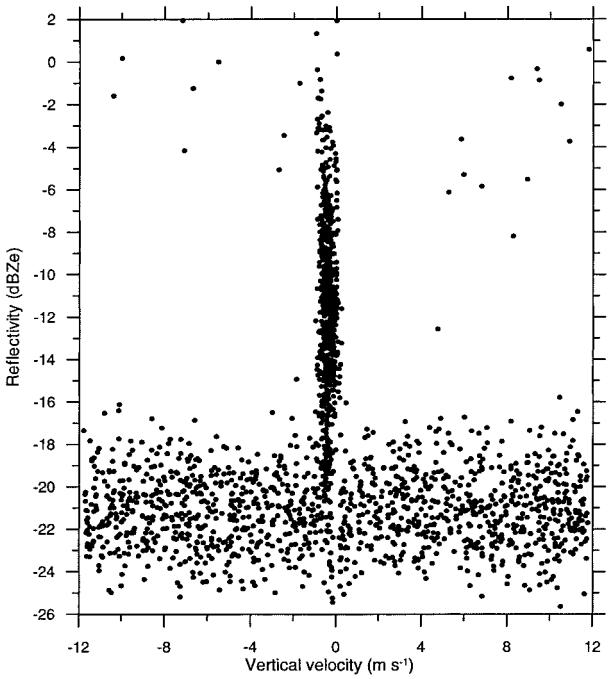

FIG. 4. S-band radar reflectivity factor as a function of vertical velocity at 7 km AGL from the time series recorded by the S-band profiler for the period 0000–2359 UTC on 8 Nov 1997.

cles are less likely to be present there. The data shown in Fig. 3 specifically satisfy these conditions, as do most of the cirrus echoes during the entire field test. In addition, these low-reflectivity targets represent a good test of the profiler's ability to detect weak clouds.

Assessing the sensitivity of the S-band profiler from the radar reflectivity measurements alone is difficult because the sensitivity of the Ka-band radar was compromised by the unavailability of its linear receiver (the Ka-band sensitivity evident in Fig. 3a is approximately −19 dBZe at 7 km). In addition, the Doppler spectral processing used with the S-band profiler produces a reflectivity measurement even when a ''true'' signal is not detectable (i.e., from a peak in the noise). However, we can use the velocities measured by the profiler and radar (Fig. 3b) to determine periods when the profiler signal dropped out. The gap in the profiler velocity time series near 2055 UTC, for example, denotes a period when the recorded velocities were outside the velocity range used to display the data. This period corresponds to an interval in Fig. 3a when the S-band dBZe values fell below the Ka-band dBZe values. To help quantify the profiler's sensitivity, we produced reflectivity–velocity displays such as the one shown in Fig. 4. The spread in velocities evident in the lower portion of the figure is associated with a random distribution of noise peaks detected in the Doppler velocity spectra. On the other hand, the distribution of velocities centered slightly to the left of 0 m s^{-1} results from atmospheric signals.

TABLE 2. S-band profiler operating parameters used during CALJET.

Parameter	Standard mode	Coupled mode	Pulse-coded mode
Pulse length (ns)	700	700	700
Interpulse period (μs)	50	50	85
Code bits	N/A	N/A	8
Range resolution (m)	105	105	105
First height sampled (km)	0.16	0.16	0.16
Maximum height sampled (km)	4.25	4.25	8.45
Unambiguous range (km)	7.5	7.5	12.75
Coherent integrations	40	40	58
FFT points	256	256	128
Spectral averages	58	58	47
Maximum radial velocity (m s^{-1})	±12.5	±12.5	±5.1
Dwell time (s)	30	30	30
Minimum detectable dBZ at 3 km	−17.2	11.5	−24.8

Based on this analysis, we estimate the S-band profiler sensitivity to be −17 dBZ at 7 km.

4. Examples

During the winter of 1997/98, the S-band profiler was part of a suite of remote and in situ sensors deployed by ETL near Cazadero, California, for the California Land-falling Jets Experiment (CALJET) (Ralph et al. 1999). The site was located on a private ranch at the crest of the coastal mountains (38.61°N, 123.22°W, 471 m above sea level). For this experiment we programmed the profiler to alternate between three operating modes: a ''standard mode'' with no pulse coding and without the coupler, a ''coupled mode'' with no pulse coding and with the coupler, and a ''pulse-coded mode'' with an 8-bit pulse code and without the coupler, resulting in a 9-dB enhancement in average power over the standard mode. Pulse coding provides a means of increasing the average transmitted power without sacrificing range resolution. The technique involves transmitting a long pulse made up of modulated or coded segments. The subsequent decoding of the received signal results in a time compression to a shorter pulse with the enhanced signal power of the longer pulse. Further details are given by Schmidt et al. (1979). The Doppler signal processing parameters associated with each of the three operating modes are listed in Table 2. Note that the dwell time for each mode is 30 s, but that consecutive measurements from a particular mode are separated by approximately 110 s, which includes the dwell times for three modes plus computer time required for processing and data storage. The pulse-coded mode was intended primarily to detect the height and depth of clouds; thus, we extended the height range, decreased the unambiguous velocity range, and increased the spectral resolution of this particular mode. The standard mode was

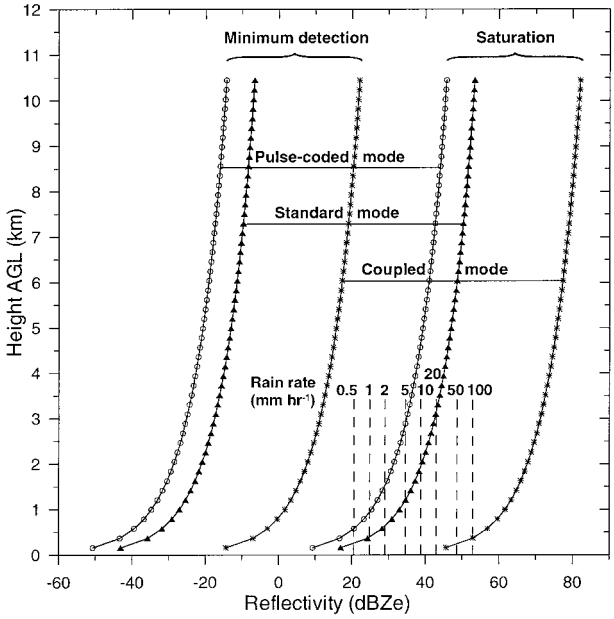

FIG. 5. Minimum detection and saturation thresholds for the ETL S-band profiler using the operating parameters listed in Table 2. The dynamic range in dB*Ze* for each operating mode is represented by a horizontal line. The dashed vertical lines indicate the reflectivities resulting from different rainfall rates assuming an exponential drop size distribution.

intended for light precipitation events and provided reflectivity measurements in the lowest eight range gates, where reflectivity measurements from the pulse-coded mode are compromised because the pulses are not fully decoded. The coupled mode extended the dynamic range of the receiver, thereby allowing the radar to make unsaturated reflectivity measurements in heavy precipitation.

Figure 5 shows the profiler's dynamic range in terms of dB*Ze* for each of the operating modes. The minimum detection thresholds were based on estimates of the noise floor determined from the CALJET observations using the method described in section 2. The saturation thresholds were calculated by assuming a dynamic range of 60 dB, which was determined by comparing standard and coupled mode reflectivity measurements of precipitation. This experimental estimate of the radar's dynamic range is 7 dB less than the theoretical range discussed in section 2. We attribute this difference to the precipitation drop size distribution observed during a radar measurement cycle, which invariably contains at least one drop of sufficient size to saturate the receiver.

To illustrate this, we calculated the radar reflectivity factor resulting from a monochromatic drop size distribution and compared it to the saturation thresholds given in Fig. 5. For the purpose of calculating number concentration, we assumed a 2.5° conical beam and used the first range gate, which yielded a range volume of approximately 4200 m^3. For a drop size distribution containing only 8-mm drops, the standard mode saturates with just one drop in the range volume, as compared to 600 drops for the coupled mode. In the case of 4-mm drops, saturation occurs with 50 drops for the standard mode and 3.8×10^4 drops for the coupled mode. In reality, a distribution of drop sizes exists. However, these simple calculations help to illustrate the difficulty associated with assigning a specific value to the saturation threshold given the heavily weighted (diameter to the sixth power) contribution of the larger drops.

Alternatively, if we knew the actual drop size distribution, we could compute the rainfall rate required to saturate the profiler. For simplicity and because we do not have access to drop size distribution measurements coincident with profiler measurements, we assume an exponential size distribution with a reflectivity–rainfall rate relation $Z = 300\,R^{1.4}$, where Z is the radar reflectivity expressed in conventional units ($mm^6\ m^{-3}$) and R is the rainfall rate in millimeters per hour. This relationship has been used routinely by the National Weather Service for quantitative precipitation estimation using the NEXRAD network. The radar reflectivity factors associated with rainfall rates ranging from 0.5 to 100 mm h^{-1} are plotted in Fig. 5. Based on this analysis, the first gate of the standard mode saturates with a rainfall rate of 0.28 mm h^{-1}, whereas the coupled mode saturates with 31.1 mm h^{-1}. However, as Doviak and Zrnić (1984) point out, the tail of an exponential size distribution extends to infinitely large drops, which is physically unrealistic. Doviak and Zrnić (1984) further explain that the reflectivity associated with a more realistic drop size distribution, in which the larger diameters are truncated, produces much smaller (by nearly 10 dBZ) reflectivity values for the same rainfall rate.

The following examples illustrate the range of observations produced using the operating modes specifically designed for CALJET. The first example shows the high sensitivity for cloud profiling obtained using the pulse-coded mode. The second example shows standard and coupled mode reflectivity measurements during periods of heavy precipitation. This example demonstrates the necessity for the added dynamic range afforded by the coupler, while at the same time it introduces the measurement ambiguity that occurs with saturation.

Time–height displays of vertical velocity and radar reflectivity factor from the pulse-coded mode measurements taken on 8 January 1998 are shown in Fig. 6. The maximum range in Fig. 6 is higher than the value listed in Table 2 because the number of range gates was reduced from 100 to 80 after 8 January to reduce data storage requirements. The speckled regions in the velocity display are measurement noise caused by low signal. Boundary layer turbulence and/or insects were sufficient on this day to produce a detectable signal in the lowest 1.5 km. Note also a thin layer of clear-air echo consisting of primarily upward motion beneath the cloud from 0500 to 1100 UTC. The cloud portion of

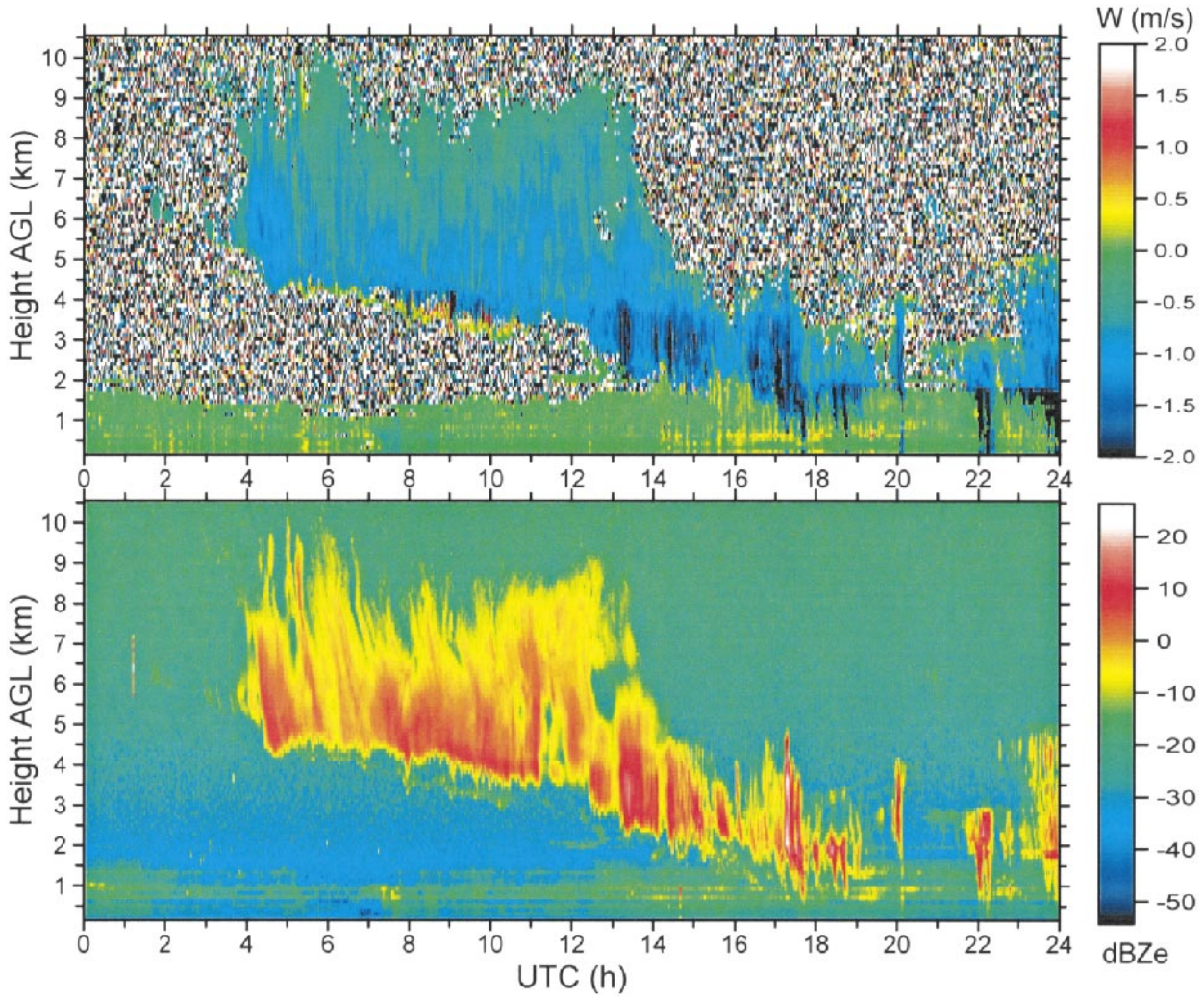

FIG. 6. Time–height images of vertical velocity (top) and dB*Ze* (bottom) recorded by the S-band profiler near Cazadero, CA, on 8 Jan 1998. The measurements were obtained using the pulse-coded operating mode described in Table 2. Speckled regions in the velocity display indicate measurement noise caused by low signal. Reflectivity banding in the lower heights results from partial decoding of the pulses.

the images depicts a descending cloud layer, which eventually produces virga after 1700 UTC, as indicated by the streaks of increased fall velocity and enhanced reflectivity in the boundary layer. The absence of measurable precipitation at the surface was confirmed by a rain gauge collocated with the radar. Details of the cloud structure are evident both in the velocity and reflectivity displays. Combining this information gives a qualitative description of the cloud microphysical profile. In addition, the CALJET S-band radar archive includes the full Doppler spectra, which can be analyzed to infer the moments of the drop size distribution (Gossard et al. 1997; Babb et al. 1999).

To demonstrate the benefit of the coupler technology, Fig. 7 compares reflectivity measurements from the standard and coupled modes taken during a storm that occurred on 19 February 1998. Above the melting layer, which is denoted in Fig. 7 by the layer of enhanced reflectivity or ''bright band,'' the reflectivity measurements from the two modes agree qualitatively. Below the melting layer, the standard mode reflectivities are substantially smaller than the coupled mode reflectivities because of receiver saturation, which is evident particularly below 500 m and near 1900 UTC, following a sharp descent in the height of the melting layer. The reduction in dB*Ze* in the lowest range gate of both modes is an artifact of the line blanker applied to prevent receiver saturation during and immediately following the transmission phase of the measurement cycle.

A more quantitative characterization of this behavior is displayed in Figs. 8 and 9. Receiver saturation does not occur in either mode for the reflectivity measurements at 2.5 km AGL (Fig. 8). The points that lie below the minimum detectable reflectivity limit for the coupled mode (dotted line) and to the left of the minimum detectable reflectivity limit for the standard mode (dashed

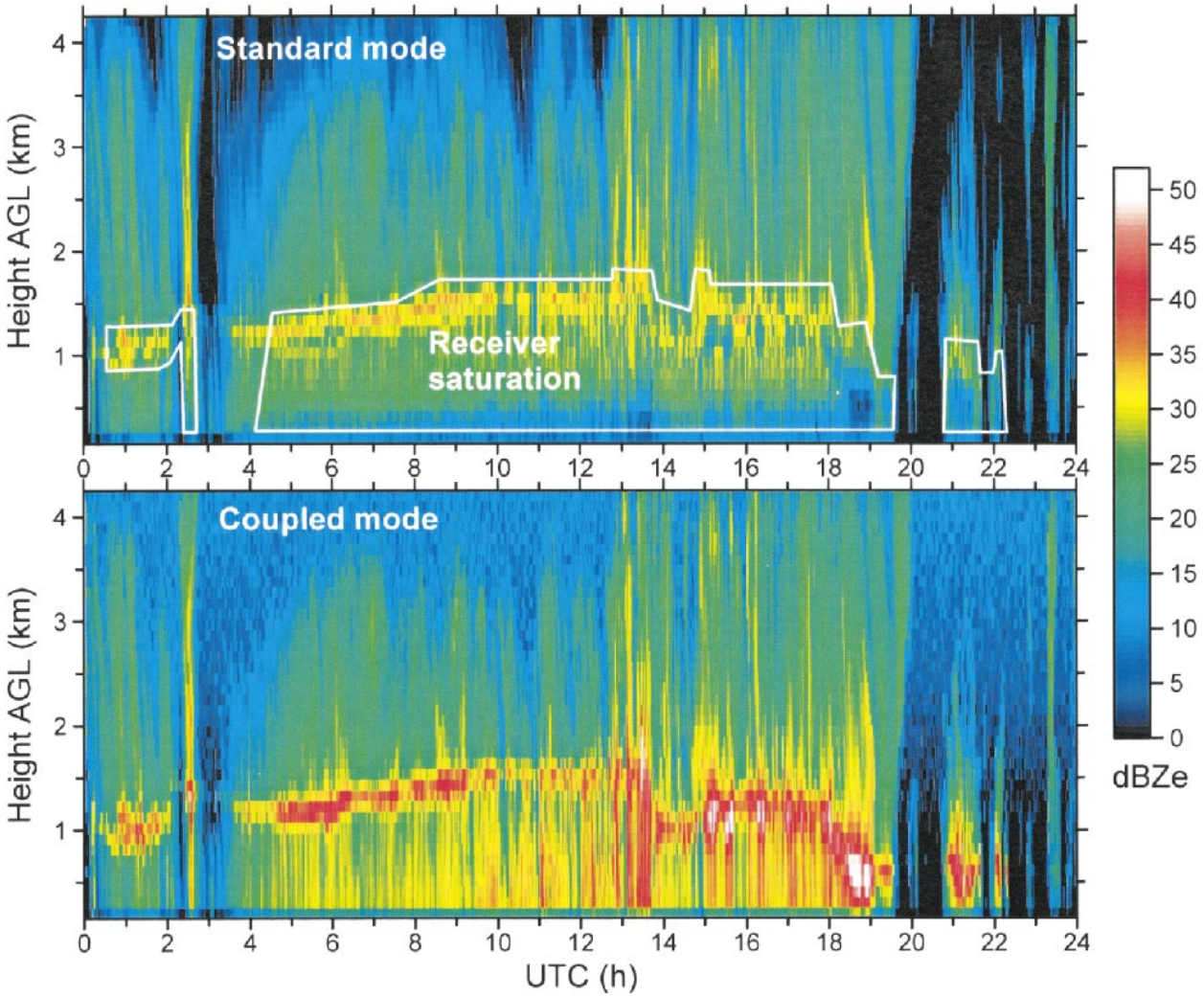

FIG. 7. Time–height images of dB*Ze* recorded by the S-band profiler near Cazadero, CA, on 19 Feb 1998 using the coupled and noncoupled operating modes. The melting layer or bright band is indicated by the layer of enhanced reflectivity rising to ~1.5 km AGL by 1200 UTC and descending to ~0.5 km AGL after 1800 UTC. White lines emphasize periods when reflectivity measurements from the standard mode were subject to receiver saturation in and below the melting layer.

line) indicate measurement noise in both modes. This cluster lies well above the 1:1 line because the noise floor for the coupled mode is higher than for the standard mode, a fact that also is evident in Fig. 7. The spread of the data points below the dotted line adds confidence to our estimate of 9.5 dB*Ze* for the coupled mode minimum detection limit at 2.5 km. The dB*Ze* values are in fair agreement above this limit, although a slight bias is apparent with higher dB*Ze* values for the coupled mode. This bias could be explained by an inaccurate coupler calibration, an undetected change in performance of the coupler from the laboratory to the field, or some other undetermined phenomenon.

The situation is different for the data at 0.5 km AGL (Fig. 9). Receiver saturation in the standard mode data is indicated by the cluster of a data points extending nearly perpendicular to the 1:1 line. This behavior demonstrates the measurement ambiguity that results as a consequence of receiver saturation. Eliminating all ambiguity in the standard mode reflectivity measurements for this case alone would require removing all reflectivities greater than 0 dB*Ze*. As a result, the effective dynamic range for the standard mode is reduced by a factor of 447 (26.5 dB).

This analysis illustrates why the coupled mode was necessary to obtain complete and accurate profiles of radar reflectivity in and below the bright band during this storm, which was typical of the winter storms that batter the California coast during a strong El Niño. In addition, these altitudes are not observed by NEXRAD radars in this and other coastal mountainous regions of California because of terrain occultation (Westrick et al. 1999). The S-band profiler data from CALJET will be used to assess and improve the performance of quan-

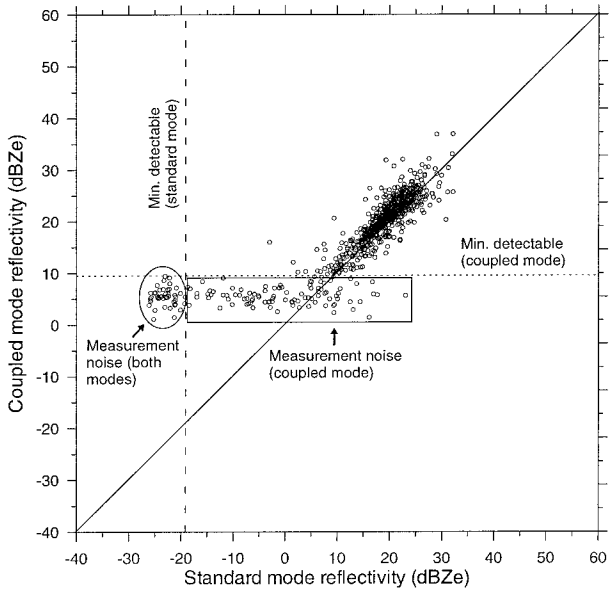

FIG. 8. Scatterplot comparing time-adjacent reflectivity measurements recorded with the standard and coupled operating modes near Cazadero, CA, on 19 Feb 1998 at 2.5 km AGL. The solid line indicates 1:1 correlation. The dashed vertical line indicates the minimum detection threshold for the standard mode taken from Fig. 5 at the appropriate altitude. The dotted line indicates the corresponding minimum detection threshold for the coupled mode. Measurement noise caused by low signal is shown by the spread of reflectivity values below the specified detection limits.

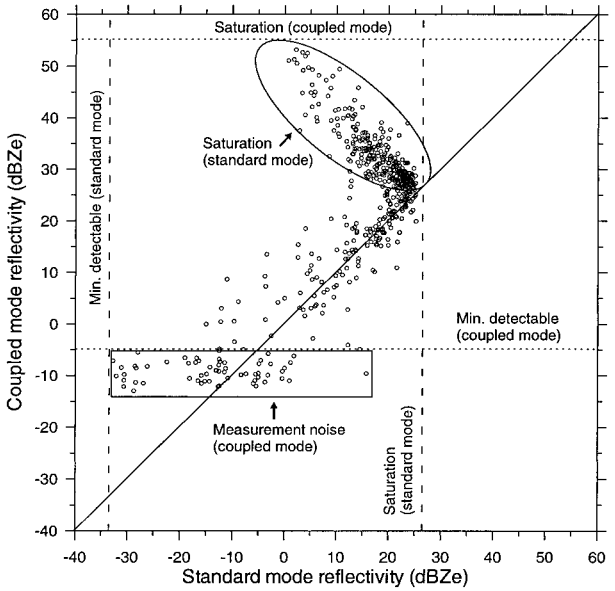

FIG. 9. As in Fig. 8, except at an altitude of 0.5 km AGL. The minimum detectable and saturation thresholds are indicated for the standard (dashed vertical lines) and coupled (dotted horizontal lines) modes. The data points enclosed by the rectangle result from coupled mode measurement noise. The data points surrounded by the oval result from correlating saturated measurements from the standard mode with unsaturated measurements from the coupled mode.

titative precipitation estimation by NEXRAD radars in one of these important flood-prone regions (Kingsmill et al. 2000).

5. Summary

The range of radar backscatter signals from hydrometeors in the atmosphere (cloud droplets to hail) can easily exceed 10 orders of magnitude. In the past, multifrequency radars or separate radars with different wavelengths have been required to measure the wide range of signals resulting from various types and intensities of clouds and precipitation. But in practice only one radar wavelength is usually available in experiments. In this paper we described a new S-band profiler with a coupler option that bridges the gap between cloud-observing radars that are highly attenuated by rain and operational weather radars, which do not suffer from severe attenuation, but generally lack the sensitivity necessary to document the structure of nonprecipitating clouds. The coupler is a simple microwave device that allows the incoming signals to be attenuated, in this case by ~30 dB, before entering the receiver. With the coupler switched off, the signals enter the receiver without attenuation. When we also took advantage of the sensitivity improvement available from pulse coding and configured the profiler to alternate sampling between a coupled mode without pulse coding and a noncoupled mode with pulse coding, a dynamic range of 96 dB was achieved without sacrificing range resolution. Using this sampling strategy, we demonstrated the distinctive ability of this observing tool to provide vertical velocity and reflectivity profile measurements during the most quiescent and most intense periods of the winter storms observed along the California coast during CALJET. The CALJET S-band profiler measurements will be used to investigate the microphysical processes associated with orographic rainfall enhancement, as well as to evaluate and improve quantitative precipitation estimation algorithms.

Acknowledgments. Funding for this research was provided by the NOAA Health of the Atmosphere Program, the NOAA U.S. Weather Research Program, and the U.S. Department of Energy Atmospheric Radiation Measurement program. The California Land-falling Jets Experiment (CALJET) was sponsored by NOAA. The authors thank three anonymous reviewers for their insightful reviews that contributed to substantial improvements in the manuscript. The authors also thank R. Kropfli and V. Zavarotny of the NOAA Environmental Technology Laboratory for reading the original manuscript and providing useful comments and suggestions. Finally, the authors express their appreciation to the many field scientists who contributed to the general success of CALJET including S. Abott, C. King, and J. Leach of the NOAA Environmental Technology Lab-

oratory, who ensured the successful operation of the S-band profiler.

REFERENCES

Babb, D. M., J. Verlinde, and B. A. Albrecht, 1999: Retrieval of cloud microphysical parameters from 94-GHz radar Doppler power spectra. *J. Atmos. Oceanic Technol.,* **16,** 489–503.

Carter, D. A., K. S. Gage, W. L. Ecklund, W. M. Angevine, P. E. Johnston, A. C. Riddle, J. S. Wilson, and C. R. Williams, 1995: Developments in UHF lower tropospheric wind profiling at NOAA's Aeronomy Laboratory. *Radio Sci.,* **30,** 997–1001.

Doviak, R. J., and D. S. Zrnić, 1984: *Doppler Radar and Weather Observations.* Academic Press, 458 pp.

Ecklund, W. L., C. R. Williams, P. E. Johnston, and K. S. Gage, 1999: A 3-GHz profiler for precipitating cloud studies. *J. Atmos. Oceanic Technol.,* **16,** 309–322.

Gossard, E. E., J. B. Snider, E. E. Clothiaux, B. Martner, J. S. Gibson, R. A. Kropfli, and A. S. Frisch, 1997: The potential of 8-mm radars for remotely sensing cloud drop size distributions. *J. Atmos. Oceanic Technol.,* **14,** 76–87.

Kingsmill, D. E., A. B. White, and F. M. Ralph, 2000: WSR-88D quantitative precipitation estimates along the northern California coast during the 1998 El Niño. Preprints, *15th Conf. on Hydrology,* Long Beach, CA, Amer. Meteor. Soc., 222–225.

Kropfli, R. A., and R. D. Kelly, 1996: Meteorological research applications of mm-wave radar. *Meteor. Atmos. Phys.,* **59,** 105–121.

——, and Coauthors, 1995: Cloud physics studies with 8 mm wavelength radar. *Atmos. Res.,* **35,** 299–313.

Moran, K. P., B. E. Martner, M. J. Post, R. A. Kropfli, D. C. Welsh, and K. B. Widener, 1998: An unattended cloud-profiling radar for use in climate research. *Bull. Amer. Meteor. Soc.,* **79,** 443–455.

Orr, B. W., and B. E. Martner, 1996: Detection of weakly precipitating winter clouds by a NOAA 404-MHz wind profiler. *J. Atmos. Oceanic Technol.,* **13,** 570–580.

Ralph, F. M., and Coauthors, 1999: The California Land-Falling Jets Experiment (CALJET): Objectives and design of a coastal atmosphere–ocean observing system deployed during a strong El Niño. Preprints, *Third Symp. on Integrated Observing Systems,* Dallas, TX, Amer. Meteor. Soc., 78–81.

Schmidt, G., R. Rüster, and P. Czechowsky, 1979: Complementary code and digital filtering for detection of weak VHF radar signals from the mesosphere. *IEEE Trans. Geosci. Electron.,* **GE-17,** 262–280.

Westrick, K. J., C. F. Mass, and B. A. Colle, 1999: The limitations of the WSR-88D radar network for quantitative precipitation measurement over the coastal western United States. *Bull. Amer. Meteor. Soc.,* **80,** 2289–2298.

White, A. B., C. W. Fairall, A. S. Frisch, B. W. Orr, and J. B. Snider, 1996: Recent radar measurements of turbulence and microphysical parameters in marine boundary layer clouds. *Atmos. Res.,* **40,** 177–221.